

# Structure of the RCK Domain from the *E. coli* K<sup>+</sup> Channel and Demonstration of Its Presence in the Human BK Channel

Youxing Jiang,<sup>\*‡||</sup> Alexander Pico,<sup>\*‡||</sup>  
Martine Cadene,<sup>†</sup> Brian T. Chait,<sup>†</sup>  
and Roderick MacKinnon<sup>\*‡§</sup>

<sup>\*</sup>Laboratory of Molecular Neurobiology  
and Biophysics

<sup>†</sup>Laboratory of Mass Spectrometry  
and Gaseous Ion Chemistry  
Rockefeller University

<sup>‡</sup>Howard Hughes Medical Institute  
New York, New York 10021

## Summary

The intracellular C-terminal domain structure of a six-transmembrane K<sup>+</sup> channel from *Escherichia coli* has been solved by X-ray crystallography at 2.4 Å resolution. The structure is representative of a broad class of domains/proteins that regulate the conductance of K<sup>+</sup> (here referred to as RCK domains) in prokaryotic K<sup>+</sup> transporters and K<sup>+</sup> channels. The RCK domain has a Rossmann-fold topology with unique positions, not commonly conserved among Rossmann-fold proteins, composing a well-conserved salt bridge and a hydrophobic dimer interface. Structure-based amino acid sequence alignments and mutational analysis are used to demonstrate that an RCK domain is also present and is an important component of the gating machinery in eukaryotic large-conductance Ca<sup>2+</sup>-activated K<sup>+</sup> channels.

## Introduction

The two major functions of ion channels are selective ion conduction (the process of ion flow across the membrane) and gating (the process of opening and closing the ion pathway) (Hille, 1992). X-ray analysis of the KcsA K<sup>+</sup> channel provides a structural basis for understanding selective ion conduction in K<sup>+</sup> channels as well as a framework for beginning to understand the gating process (Doyle et al., 1998). Because the KcsA channel architecture is representative of a very broad set of cation channels—including K<sup>+</sup>, Na<sup>+</sup>, and Ca<sup>2+</sup> channels; cyclic nucleotide-gated channels; and glutamate receptors—a common theme in ion channel gating may be anticipated.

The KcsA architecture is referred to as an inverted teepee because of its arrangement of four inner helices (Figure 1A). The inner helices form a right-handed bundle that constricts the pore diameter near the intracellular membrane surface (red cylinders). This arrangement of helices implies that the pore can be gated through inner-helix movements, and mutational analysis of the related Shaker voltage-dependent K<sup>+</sup> channel supports this no-

tion (Liu et al., 1997; Yellen, 1998). Recent electron paramagnetic resonance spectroscopic data confirm that the inner helices do indeed undergo movements upon KcsA channel gating (Cortes and Perozo, 1997; Perozo et al., 1999).

The fundamental stimulus that controls ion channel gating differs from one channel to the next. The stimulus differs even among K<sup>+</sup> channels; some are gated by changes in membrane voltage, whereas others respond to the binding of a ligand such as Ca<sup>2+</sup> or a G protein subunit. But it is likely that these different stimuli bring about a similar conformational change in the pore, presumably movements of the inner helices, in order to gate the channel. This suggestion is fortified by the observation that many inverted teepee ion channels contain a domain in the position corresponding to the C-terminal end of the inner helix (Finn et al., 1996; Stumpe et al., 1996; Tucker et al., 1997; Derst and Karschin, 1998; Xia et al., 1998; Keen et al., 1999) (Figure 1). These domains, adjacent to the base of the inner helix bundle, are well positioned to control the open–closed state of the pore through ligand binding–induced conformational changes.

The majority of prokaryotic K<sup>+</sup> channels share a common C-terminal domain immediately following their inner helix (Figure 1B, i and ii). This domain is homologous to the pair of domains that constitute TrkA, the intracellular component of the Trk system of prokaryotic K<sup>+</sup> transporters (Schlosser et al., 1993; Parra-Lopez et al., 1994; Derst and Karschin, 1998; Durell et al., 1999). We refer to the domains collectively as RCK domains for their apparent role in regulating the conductance of K<sup>+</sup> in prokaryotic K<sup>+</sup> transporters and K<sup>+</sup> channels. The RCK domains found in TrkA and many of the prokaryotic K<sup>+</sup> channels contain the NAD binding glycine motif, GXGXXG...D, indicating a particular ligand binding function (Bellamacina, 1996). The glycine motif, however, is not conserved in a significant subset of the prokaryotic K<sup>+</sup> channels, indicating that the RCK domain in some cases may serve a function other than binding a nucleotide cofactor. In particular, where the RCK domain is found in prokaryotic K<sup>+</sup> channels containing six transmembrane segments per subunit (e.g., the *Escherichia coli* K<sup>+</sup> channel; Milkman, 1994), the glycine motif and presumably the NAD binding function are uniformly absent.

Remarkably, RCK domains are also found in a subfamily of eukaryotic K<sup>+</sup> channels, the large-conductance Ca<sup>2+</sup>-activated K<sup>+</sup> channels (BK channels; Figure 1B) (Stumpe et al., 1996). BK channels exhibit the dual function of gating in response to membrane voltage as well as intracellular Ca<sup>2+</sup> levels. BK channels have seven membrane-spanning segments per subunit, forming the pore and voltage sensor, and an intracellular C terminus that is important for Ca<sup>2+</sup>-induced gating (Schreiber and Salkoff, 1997).

In this paper, we present the x-ray crystal structure of the RCK domain from the *E. coli* K<sup>+</sup> channel. Through structure-based alignment of amino acid sequences and mutational analysis of human BK channels expressed

<sup>§</sup>To whom correspondence should be addressed (e-mail: mackinn@rockvax.rockefeller.edu).

<sup>||</sup>These authors contributed equally to this work.

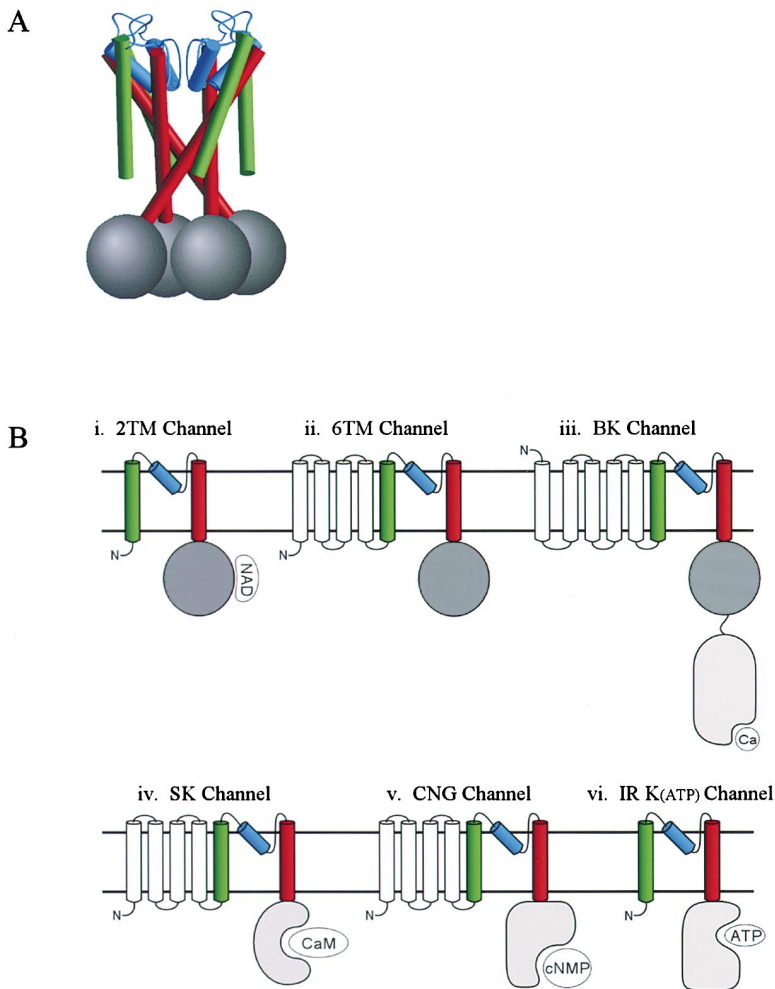


Figure 1. A Visual Argument for Channel Regulation by C-Terminal Cytoplasmic Domains

(A) Depiction of the aperture formed by inner helices (red) of the tetrameric KcsA K<sup>+</sup> channel with a nondescript C-terminal domain (gray).

(B) Example topologies of varied subfamilies of K<sup>+</sup> channels: (i) prokaryotic K<sup>+</sup> channels with two transmembrane (TM) helices and a putative NAD binding RCK domain (shaded); (ii) prokaryotic K<sup>+</sup> channels with six TM helices and an RCK domain (e.g., *E. coli* Kch); (iii) eukaryotic large-conductance Ca<sup>2+</sup>-activated K<sup>+</sup> channels (BK) with a homologous RCK domain and C-terminal Ca<sup>2+</sup> binding domain; (iv) eukaryotic small-conductance Ca<sup>2+</sup>-activated K<sup>+</sup> channels (SK) with a calmodulin binding domain; (v) eukaryotic cyclic nucleotide-gated channels (CNG) with a cNMP binding domain; and (vi) eukaryotic ATP-sensitive inward rectifier K<sup>+</sup> channels (Kir6.1 and 6.2) with an ATP binding domain.

in *Xenopus* oocytes, we demonstrate that an equivalent RCK domain is also present in BK channels and participates in channel gating.

## Results

### RCK Domain Family

A survey of prokaryotic K<sup>+</sup> channels was conducted using the core K<sup>+</sup> channel region as a query sequence in a database search using BLAST and PSI-BLAST (Altschul et al., 1997). BLAST was used in manual iteration, utilizing hits from one search as query sequences for later searches until the list converged. The criteria for including a sequence in the list were as follows. First, the sequence must contain two to six predicted membrane-spanning segments according to the DAS-TM prediction server (Cserzo et al., 1997); and second, between the last two transmembrane helices there must be a recognizable K<sup>+</sup> channel signature sequence with only conservative substitutions. A subset of sequences was used in later rounds of database searches to identify homologs of the conserved intracellular C-terminal domain of prokaryotic K<sup>+</sup> channels and to define the RCK family of domains. The results included TrkA proteins, numerous "hypothetical proteins" in prokaryotes, and

segments of the intracellular C terminus of eukaryotic BK channels. In Figure 2, representative sequences of RCK domains from eukaryotic BK channels, prokaryotic K<sup>+</sup> channels, and TrkA proteins were aligned using ClustalW (Thompson et al., 1994) and knowledge of the *E. coli* K<sup>+</sup> channel RCK domain structure.

### Structure of the *E. coli* K<sup>+</sup> Channel RCK Domain

The RCK domain from the *E. coli* K<sup>+</sup> channel C terminus, corresponding to amino acids Met-240 to Lys-417, was expressed in *E. coli* as a soluble, hexahistidine fusion protein. Following purification, removal of the hexahistidine element, and crystallization, the structure was determined through a multiwavelength anomalous dispersion experiment with selenomethionine substituted protein (space group C222<sub>1</sub>, two molecules per asymmetric unit) and refined (30–2.4 Å, R<sub>free</sub> 26.0%). The structure of a second crystal form (P4<sub>1</sub>, two molecules per asymmetric unit) was determined by molecular replacement using the first structure as a search model and refined (30–2.4 Å, R<sub>free</sub> 23.6%). The refined structures of the two crystal forms comprise amino acids His-241 to Asn-393 of the *E. coli* K<sup>+</sup> channel (Table 1).

The RCK domain is an α/β protein, the core of which forms a Rossmann fold (residues 241–365), with two α

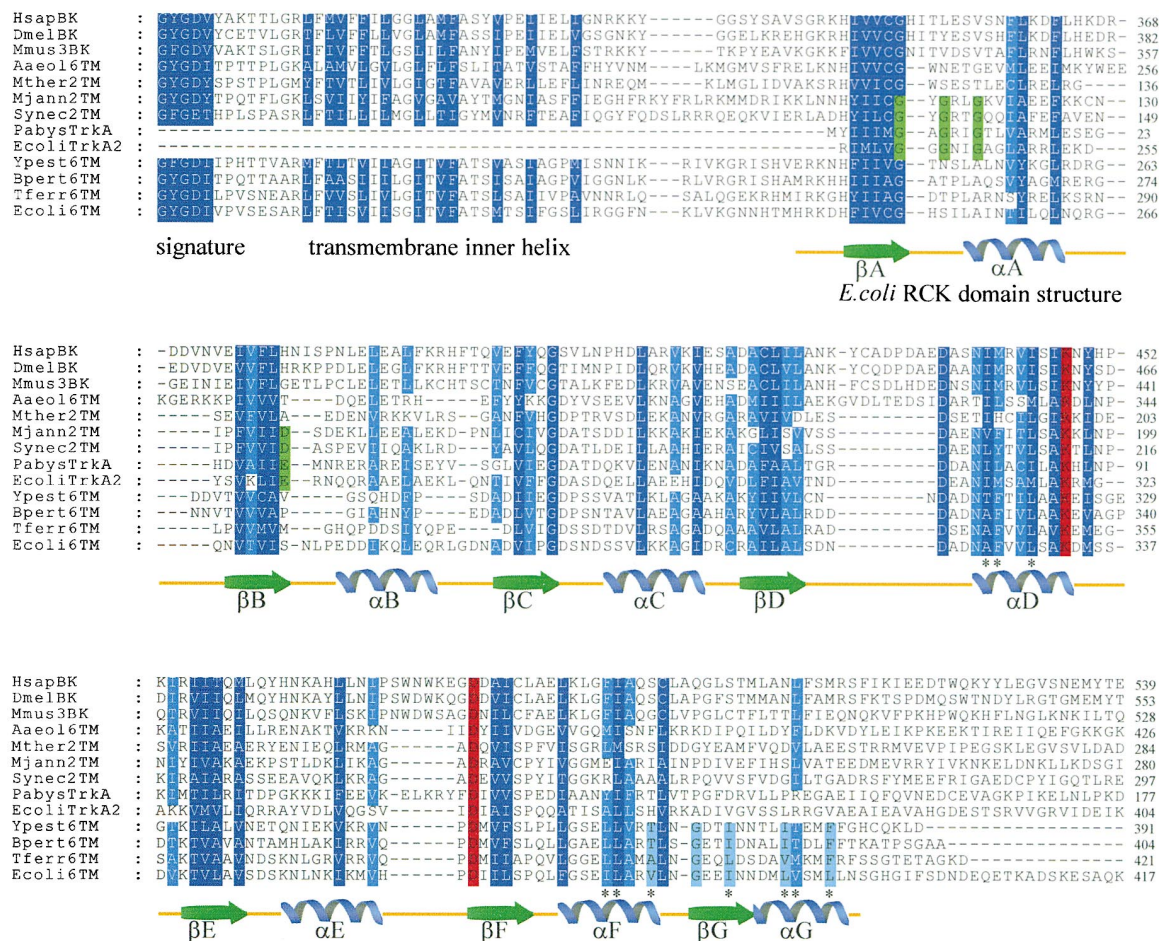


Figure 2. Multiple Sequence Alignment of Representative Eukaryotic BK Channels, Prokaryotic K<sup>+</sup> Channels, and TrkA Proteins Sharing the RCK Domain

The alignment begins at the K<sup>+</sup> channel signature, GYGD (which forms the selectivity filter), passes through the inner helix, and covers the RCK domain region through to the end of the *E. coli* K<sup>+</sup> channel sequence. Below the alignment, the elements of secondary structure are indicated pictorially as determined by the crystal structure of the *E. coli* RCK domain. The sequence similarity tapers off at  $\alpha$ F. In the conservation pattern, dark blue indicates 100% and blue 85%, using similarity groups DE, KR, GP, and LIVAMCFYT. Green highlights the NAD binding glycine motif, red highlights salt bridging positions, and light blue highlights interface positions uniquely conserved among the set of six-transmembrane prokaryotic K<sup>+</sup> channels. Asterisks denote the hydrophobic positions that form dimer interfaces at  $\alpha$ D and at  $\alpha$ F,  $\beta$ G, and  $\alpha$ G.

Abbreviations: HsapBK, human BK channel, Hslo (*Homo sapiens* Gl:2570854); DmelBK, *Drosophila* BK channel, Dslo (*Drosophila melanogaster* Gl:7301192); Mmus3BK, mouse BK channel, Msl03 (*Mus musculus* Gl:6680542); Aaeol6TM, six-transmembrane prokaryotic K<sup>+</sup> channel (*Aquifex aeolicus* Gl:7520841); Mther2TM, two-transmembrane prokaryotic K<sup>+</sup> channel (*Methanobacterium thermoautotrophicum* Gl:7482789); Mjann2TM, two-transmembrane prokaryotic K<sup>+</sup> channel (*Methanococcus jannaschii* Gl:2493595); Synec2TM, two-transmembrane prokaryotic K<sup>+</sup> channel (*Synechocystis* sp. Gl:7447543); PabysTrkA, TrkA protein (*Pyrococcus abyssii* Gl:7450648); EcoliTrkA2, TrkA protein, domain 2 (*E. coli* Gl:136235); Ypest6TM, six-transmembrane prokaryotic K<sup>+</sup> channel (*Yersinia pestis* Sanger\_632); Bpert6TM, six-transmembrane prokaryotic K<sup>+</sup> channel (*Bordetella pertussis* Sanger\_520); Tferr6TM, six-transmembrane prokaryotic K<sup>+</sup> channel (*Thiobacillus ferrooxidans* TIGR\_2975); Ecoli6TM, six-transmembrane prokaryotic K<sup>+</sup> channel (*E. coli* Gl:400124).

helices ( $\alpha$ A and  $\alpha$ B) on one side of a six stranded parallel  $\beta$  sheet ( $\beta$ A to  $\beta$ F) and three  $\alpha$  helices ( $\alpha$ C,  $\alpha$ D and  $\alpha$ E) on the other (Figure 3). The remaining residues, 366 to 393, form a helix-strand-helix structure that extends from one edge of the parallel  $\beta$  sheet ( $\alpha$ F- $\beta$ G- $\alpha$ G).

The Rossmann fold is a very common structural motif found in many different enzymes and ligand binding proteins (Branden and Tooze, 1991). The active site or ligand binding site is always located at the C-terminal ends of the parallel  $\beta$  strands (Figure 3B), where amino acids from the loops connecting the  $\beta$  strands to the  $\alpha$  helices are able to coordinate a small molecule or metal ion. Typically, the ligand serves as a substrate or cofac-

tor in enzyme catalysis. In the case of integrin domain A, a bound Mg<sup>2+</sup> ion is postulated to mediate protein-protein interactions (Lee et al., 1995). Rossmann-fold domains therefore are versatile in their function but have in common the potential to bind a small molecule or metal ion. A ligand is not present in our crystal structures of the *E. coli* RCK domain; however, we think it is very possible that a functionally important ligand does exist.

Analysis of protein packing within the crystal lattice reveals two interesting ways that pairs of *E. coli* RCK domains interact with each other and are related by 2-fold rotational axes. One "dimer" pair is defined by a noncrystallographic 2-fold axis and the other by a

Table 1. Data and Refinement Statistics

Data and Phasing Statistics					
Crystal Form	C222 <sub>1</sub>	C222 <sub>1</sub>	C222 <sub>1</sub>	C222 <sub>1</sub>	P4 <sub>1</sub>
Source	CHES F2	CHES F2	CHES F2	CHES F2	NLSL X25
Data set	Data I	Data I	Data I	Data I	
Wavelength (Å)	$\lambda_1 = 0.9792$	$\lambda_2 = 0.9788$	$\lambda_3 = 0.9633$	$\lambda = 0.9792$	$\lambda = 1.100$
Resolution (Å)	30–2.8	30–2.8	30–2.8	30–2.4	30–2.4
R <sub>sym</sub> (%) <sup>a</sup>	5.9 (25.3)	5.8 (25.6)	5.8 (25.0)	4.7 (24.7)	8.6 (29.2)
Redundancy <sup>b</sup>	3.7	3.7	3.7	5.0	4.8
Completeness (%)	98 (99.3)	97.9 (99.3)	97.9 (98.8)	74.0 (77.7)	99.5 (96.3)
R <sub>culis</sub> (anomalous) <sup>c</sup>	0.81	0.78	0.84		
R <sub>culis</sub> (dispersive) <sup>d</sup>	–	0.86	0.78		molecular replacement
Overall FOM <sup>e</sup>		0.47			
Refinement Statistics					
Resolution (Å)		30–2.4 <sup>h</sup>			30–2.4
Number of reflections		14,208			17,912
Number of atoms		protein/water	2260/67		protein/water
R factors (%) (all data) <sup>f</sup>		R <sub>work</sub> /R <sub>free</sub>	21.5/26.0		R <sub>work</sub> /R <sub>free</sub>
Rmsd of bond <sup>g</sup>		length/angle	0.008 Å/1.33°		length/angle
					2263/57
					20.8/23.6
					0.008 Å/1.30°

<sup>a</sup>R<sub>sym</sub> =  $\sum |I_i - \langle I_i \rangle| / \sum I_i$ , where  $\langle I_i \rangle$  is the average intensity of symmetry equivalent reflections. Numbers in parentheses are statistics for last resolution shell. Same for completeness.

<sup>b</sup>Redundancy = total measurements/unique reflections. Bijvoets pairs were treated as separate reflections in MAD data set.

<sup>c</sup>R<sub>culis</sub> (anomalous) =  $\sum |\Delta_{\text{ano}}(\text{obs}) - \Delta_{\text{ano}}(\text{cal})| / \sum \Delta_{\text{ano}}(\text{obs})$  for acentric reflections, where  $\Delta_{\text{ano}}$  is the anomalous difference.

<sup>d</sup>R<sub>culis</sub> (dispersive) =  $\sum |\Delta_{\text{iso}}(\text{obs}) - \Delta_{\text{iso}}(\text{cal})| / \sum \Delta_{\text{iso}}(\text{obs})$  for centric reflections, where  $\Delta_{\text{iso}}$  is the isomorphous difference between native and derivative. Data of  $\lambda_1$  were used as native.

<sup>e</sup>FOM = figure of merit.

<sup>f</sup>R factor =  $\sum |F(\text{obs}) - F(\text{cal})| / \sum F(\text{obs})$ , 10% of the data that were excluded in refinement were used in the R<sub>free</sub> calculation.

<sup>g</sup>Rmsd = root-mean-square deviation.

<sup>h</sup>Merged data between Data II and  $\lambda_1$  of Data I were used for refinement.

crystallographic 2-fold axis. There are reasons to suspect that the contact interfaces involved in both of these “dimer” pairings represent something more than crystallographic coincidence and imply biologically relevant protein–protein interactions. The first interface is formed by the helix–strand–helix structure ( $\alpha$ F– $\beta$ G– $\alpha$ G) attached to the Rossmann fold, comprising amino acids 366 to 393 (Figure 4A). This interface is hydrophobic, well packed, and contains 1800 Å<sup>2</sup> of buried surface area. These features, together with preliminary experiments showing that mutation of the interface profoundly affects channel expression (data not shown), imply biological relevance for the *E. coli* K<sup>+</sup> channel. This contact surface holds the two Rossmann folds together with their potential ligand binding sites facing each other across an interdomain cleft (Figure 4A). Interestingly, a similar arrangement of two Rossmann fold-like domains is observed in the bacterial periplasmic amino acid binding protein LIVBP (Sack et al., 1989). In LIVBP the two halves are contained within a single protein in which a connector known as the “hinge region” forms a pseudo-2-fold axis relating the domains (Figure 4B). A free amino acid—leucine, isoleucine, or valine—binds in the deep intervening cleft. Thus, nature achieved similar orientations of two Rossmann fold-like domains by very different means in the *E. coli* RCK domain and LIVBP. The finding of a 2-fold arrangement of Rossmann folds on a K<sup>+</sup> channel is intriguing in light of the recent evidence that LIVBP is a good structural model for the Zn<sup>2+</sup> binding regulatory domain present on another class of ion channels, the eukaryotic glutamate receptors (Paoletti et al., 2000). This dimer interface, however, is a unique feature of the RCK domains found in the *E. coli* K<sup>+</sup> channel and a few other six-transmembrane prokaryotic K<sup>+</sup> channels (Figure 2, asterisks above  $\alpha$ F– $\beta$ G– $\alpha$ G) and is not conserved in two-transmembrane prokaryotic K<sup>+</sup> channels, K<sup>+</sup> transporters, or eukaryotic BK channels.

The second interface is also hydrophobic, but less extensive in area (~860 Å<sup>2</sup>). The dimer interaction is formed by hydrophobic residues (Ala-326, Phe-327, and Leu-330) on the external face of  $\alpha$ D (Figure 3B). Sequence alignment shows that these surface residues are conserved as hydrophobic in all RCK domains, including those of prokaryotic K<sup>+</sup> channels, K<sup>+</sup> transporters, and eukaryotic BK channels (Figure 2, asterisks above  $\alpha$ D) but are not generally a conserved feature of Rossmann-fold proteins. Mutational analyses show that disruption of this dimer interface abolishes the expression of the *E. coli* K<sup>+</sup> channel in *E. coli* host strains and the expression of BK channels in *Xenopus* oocytes, which suggests that this dimer interface may be important for the function of RCK domains.

Another feature of the *E. coli* RCK domain structure is the salt bridge between Lys-333 at the C terminus of  $\alpha$ D and Asp-360 at the loop connecting  $\alpha$ E and  $\beta$ F (Figure 3B). Sequence alignment shows that these two positions are conserved in all RCK domains (Figure 2).

#### Evidence for an RCK Domain in BK Channels

The sequence identity between BK and prokaryotic RCK domains is less than 20%, well below the threshold for accurate structure modeling (i.e., >30%–40% sequence identity) (Sanchez and Sali, 1998). It was therefore necessary to seek additional evidence for relevance of the conserved sequence to the hypothesized conservation of structure. To this end, it was evident that conserved residues are not distributed randomly but correlate strongly with secondary structural elements. Further, the conservation pattern among the prokaryotic sequences is consistent with the pattern found in BK channel sequences; in other words, there are very few positions (4 out of 55) that are conserved in the prokaryotic set of sequences that are not conserved in the BK set.

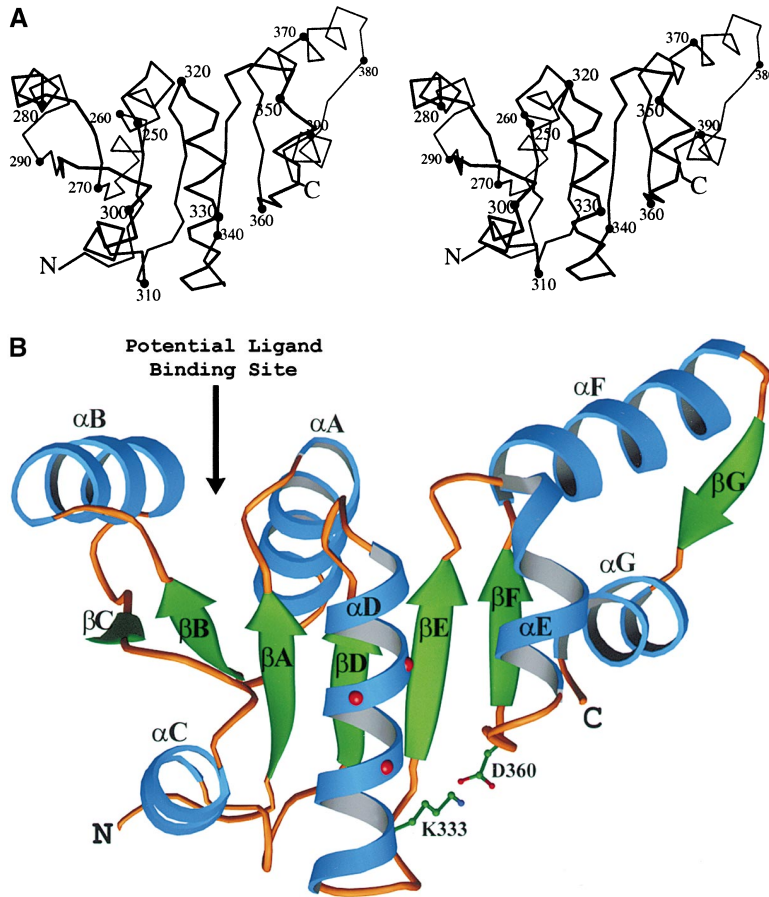


Figure 3. Structure of *E. coli* K<sup>+</sup> Channel RCK Domain

(A) Stereo view of the C<sub>α</sub> trace of the *E. coli* K<sup>+</sup> channel RCK domain.

(B) Ribbon diagram of the *E. coli* K<sup>+</sup> channel RCK domain in the same orientation as (A). The potential ligand binding site was labeled based on the known structures of ligand binding proteins with a Rossmann fold. The side chains of K333 and D360 form a salt bridge and are conserved in all RCK domains. The three red spheres on the external face of αD indicate the positions of conserved hydrophobic residues (Ala-326, Phe-327, and Leu-330) that form one of the dimer interfaces.

Finally, two specific amino acids, conserved in the prokaryotic set, that form a salt bridge in the *E. coli* RCK domain structure are also conserved in the BK sequences (Figure 2).

To test the structural prediction that Lys-448 and Asp-481 form a salt bridge in the human BK channel, we studied wild-type and mutant BK channels using an electrophysiological assay (Figure 5). The BK channels are opened by electrical depolarization of the cell membrane as well as by binding of Ca<sup>2+</sup> to a site on the

intracellular side of the channel. The intracellular Ca<sup>2+</sup> levels govern the midpoint of the voltage-activation curve; as Ca<sup>2+</sup> concentration is raised, less membrane depolarization is required to open the channels (Figure 5C). Figure 5D graphs the relationship between the midpoint voltage (voltage at which the channels have a 50% probability of being open) times the gating valence, z, and the intracellular Ca<sup>2+</sup> concentration for wild-type and mutant channels. To a first approximation, the mutations shift the position of zV<sub>50</sub> in a Ca<sup>2+</sup>-independent

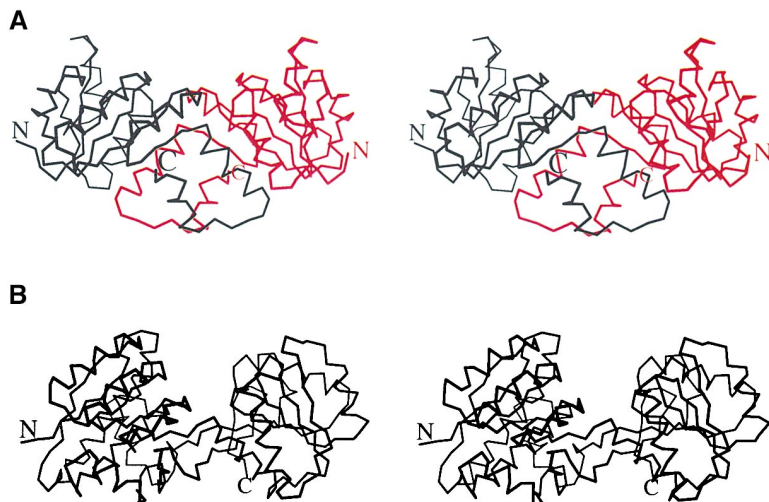


Figure 4. Comparison between the *E. coli* K<sup>+</sup> Channel RCK Domain Dimer and the *E. coli* LIV Binding Protein

(A) Stereo view of the C<sub>α</sub> trace of the *E. coli* K<sup>+</sup> channel RCK domain dimer. Subunits are black and red.

(B) Stereo view of the C<sub>α</sub> trace of the *E. coli* LIV binding protein.

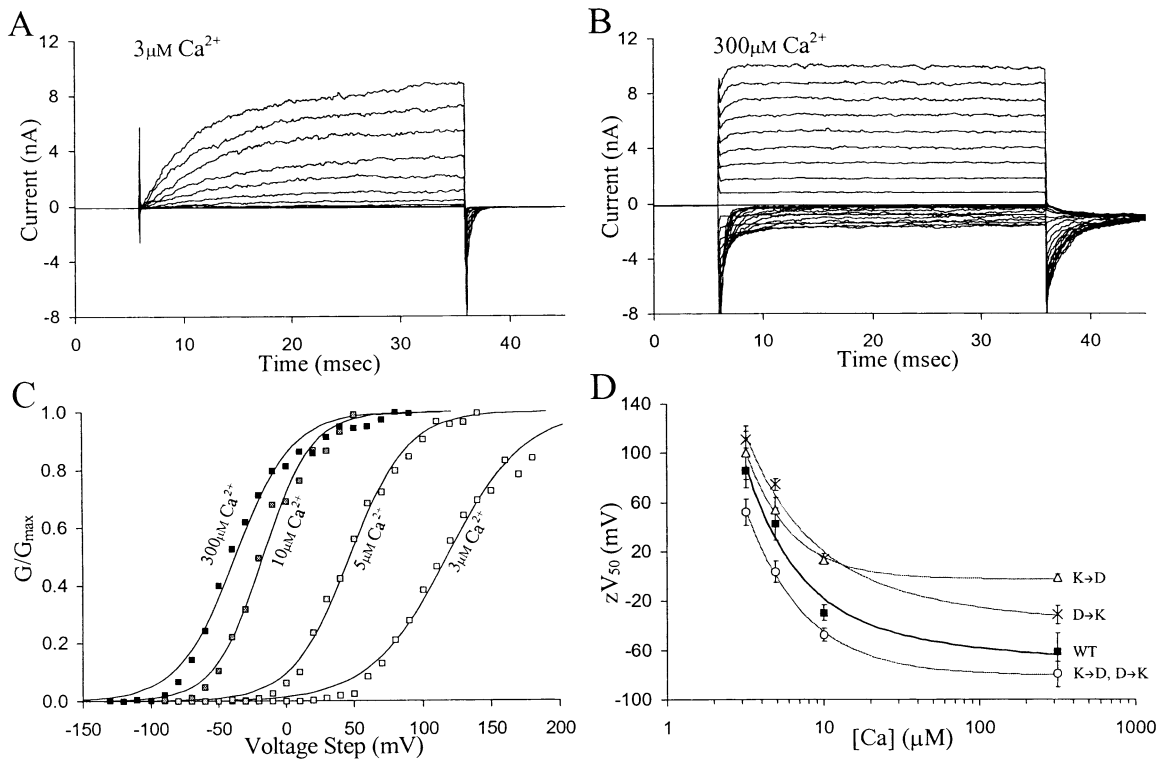


Figure 5. Electrophysiological Study of Wild-Type and Mutant Human BK Channels

(A) Family of current traces from a voltage-clamped inside-out patch of  $\sim 400$  channels in a bath solution containing  $3 \mu\text{M Ca}^{2+}$ . Voltage steps ranged from  $-40 \text{ mV}$  to  $+120 \text{ mV}$  in  $10 \text{ mV}$  increments.

(B) Current traces from the same patch in  $300 \mu\text{M Ca}^{2+}$ . Voltage steps ranged from  $-150 \text{ mV}$  to  $+90 \text{ mV}$  in  $10 \text{ mV}$  increments.

(C) Open probability curves for the same patch over a range of voltage steps at four different free calcium ion concentrations:  $3 \mu\text{M}$  (open squares),  $5 \mu\text{M}$  (light shaded squares),  $10 \mu\text{M}$  (dark shaded squares), and  $300 \mu\text{M}$  (closed squares). Conductances ( $G$ ) were measured at tail currents  $200 \mu\text{s}$  after a tail step in voltage (typically to  $-60 \text{ mV}$ ) and normalized by observed maximum conductances ( $G_{\text{max}}$ ). Data points were fit with the Boltzmann equation  $G = G_{\text{max}} / (1 + \exp[-(x - V_{50}) \times zF/RT])$ , where  $V_{50}$  is the midpoint voltage,  $z$  is the gating valence,  $F$  is Faraday's constant,  $R$  is the gas constant, and  $T$  is temperature.

(D) The  $\text{Ca}^{2+}$  activation profile is shown by graphing  $zV_{50}$  against  $[\text{Ca}^{2+}]$  concentration (Cui and Aldrich, 2000). The profile is shown for wild-type (WT, closed squares, bold line) and mutant BK channels. K→D denotes K448D (open triangles), D→K denotes D481K (crosses), and K→D, D→K denotes the double mutant K448D, D481K (open circles). Upward shifts were observed for the single mutants (K→D and D→K), whereas the double mutant caused a downward shift in the  $\text{Ca}^{2+}$  activation profile. Each data point represents the average of three independent data sets (except in the case of K→D, for which each point is the mean of two data sets); error bars indicate the standard deviation.

manner (i.e., curves are displaced along the y axis). If either position of the proposed salt bridge pair is mutated singly (Lys to Asp or Asp to Lys), the curve is displaced upward relative to that for the wild-type channel. However, if both positions are mutated simultaneously (Lys to Asp and Asp to Lys) the curve is more similar to wild-type than is that of either single mutant alone. Through such double-mutant cycle analysis, we conclude that the mutations do not have independent effects on channel function. The observation that a double charge swap has a smaller effect than either single mutation alone is compatible with the hypothesis that Lys-448 and Asp-481 form a salt bridge in the BK channel and that the BK channel contains an RCK domain on its intracellular C terminus.

## Discussion

Sequence information and functional analysis of a variety of ion channels support the notion that ligand binding domains attached to the inner helices control opening

and closing of the ion pathway. Perhaps the best-studied examples are the monovalent cation channels gated by intracellular cyclic AMP and cyclic GMP. Though not selective for  $\text{K}^+$  ions, the cyclic nucleotide-gated channels are related to  $\text{K}^+$  channels but have an incomplete  $\text{K}^+$  channel signature sequence. A cyclic nucleotide binding domain is present on the C-terminal end of the transmembrane segment corresponding to the  $\text{K}^+$  channel inner helix; cyclic nucleotides bind at physiological concentrations to control channel gating (Finn et al., 1996; Zagotta and Siegelbaum, 1996). Many  $\text{K}^+$  channels have different ligand binding domains in the corresponding position, as summarized in Figure 1B. The emerging picture is pleasingly simple: ligand binding induces domain conformational changes that apparently exert strain on the inner helices, causing the pore to open.

The intracellular C-terminal domain of the *E. coli*  $\text{K}^+$  channel is structurally representative of a broad class of proteins/domains that are involved in regulating  $\text{K}^+$  conductance, the RCK domains. RCK domains are

found not only in the majority of prokaryotic K<sup>+</sup> channels but also in prokaryotic K<sup>+</sup> transport systems as peripheral membrane subunits (TrkA) and in eukaryotic BK channels. The alignment of RCK domain sequences and the crystal structure of the *E. coli* RCK domain reveal three general features of the RCK domain: the domain has a Rossmann-fold topology, a salt bridge between a positively charged residue (Arg or Lys) at the C terminus of  $\alpha$ D and a negatively charged residue (Asp or Glu) at the loop connecting  $\alpha$ E and  $\beta$ F, and a hydrophobic dimer interface on the external face of  $\alpha$ D. How these domains regulate transport or channel activity is unknown. In certain cases, where a glycine motif is conserved in the ligand binding loops (Figure 2), NAD binding is implicated, but the glycine motif is not a universal feature.

The RCK domains of the *E. coli* K<sup>+</sup> channel and other six-transmembrane prokaryotic K<sup>+</sup> channels have a unique feature that is not conserved in other RCK domains. They possess an extended helix-strand-helix generating a second, very extensive dimer interface. The two Rossmann folds of the *E. coli* RCK dimer are arranged in a manner resembling the two halves of the amino acid binding protein LIVBP (Sack et al., 1989). This implicates a possible ligand binding site between the two RCK domains, an alternative to the cleft indicated in Figure 3B. A ligand binding site formed by two domains is observed in glutamate receptor channels. Until we have further structural information, we do not wish to speculate on how the RCK domains of K<sup>+</sup> channels are arranged with respect to the ion pathway, or how they are energetically coupled to it. However, we suggest that they serve a ligand binding function that underlies channel gating.

One important class of eukaryotic K<sup>+</sup> channels, the BK channels, also contains the RCK domain. The BK channels underlie numerous important physiological processes, but it is as much the challenge of understanding their large conductance and dual responsiveness to membrane voltage and Ca<sup>2+</sup> that has made the BK channels a favorite subject of study. Efforts to understand the Ca<sup>2+</sup> activation have focused on a postulated serine protease-like domain with Ca<sup>2+</sup> binding capability located at the intracellular C terminus (Moss et al., 1996). The RCK domain resides between the pore-lining inner helix and the Ca<sup>2+</sup> binding region, and mutations described here show that perturbations of the RCK domain modify the gating response of the channel to intracellular Ca<sup>2+</sup>. We postulate that the RCK domain is an important component of the Ca<sup>2+</sup> gating mechanism, and the structure presented here provides a starting model for further studies of this process.

## Experimental Procedures

### Protein Purification and Crystallization

The RCK domain of the *E. coli* K<sup>+</sup> channel (Met-240 to Lys-417) was cloned into the pET28b(+) expression vector using NcoI/XhoI restriction sites with a thrombin cleavage site between the C-terminal His tag and the protein. Protein was overexpressed in the *E. coli* BL21(DE3) cell strain. Cells were grown in LB medium at 37°C and induced with 0.4 mM IPTG. Supernatant of the cell lysate was loaded onto a Talon Co<sup>2+</sup> affinity column (Clontech). After washing the resin with buffer containing 10 mM imidazole, the protein was eluted with buffer containing 300 mM imidazole. After removing the His tag by

thrombin cleavage, the protein was further purified with a Superdex 200 gel-filtration column. For selenomethionine substituted protein, the *E. coli* B834(DE3) cell strain was used in overexpression and the cells were grown in minimal medium.

Crystals grew at 20°C with the use of the vapor diffusion method in sitting drops. Protein at 15–20 mg/ml in 10 mM Tris-HCl (pH 8.0) and 10 mM NaCl was mixed with an equal volume of reservoir solution. The C222<sub>1</sub> crystal form was grown over a reservoir solution of 12%–18% MPD and 100 mM Na acetate (pH 5.0) and has a unit cell of  $a = 75.62 \text{ \AA}$ ,  $b = 108.65 \text{ \AA}$ ,  $c = 95.53 \text{ \AA}$ , and  $\alpha = \beta = \gamma = 90^\circ$ . The P<sub>4</sub> crystal form was grown over a reservoir solution of 10% PEG4000, 1–1.5 M NaCl, and 100 mM Tris-HCl (pH 8.0–8.5) and has a unit cell of  $a = b = 65.51 \text{ \AA}$ ,  $c = 110.24 \text{ \AA}$ , and  $\alpha = \beta = \gamma = 90^\circ$ .

### Data Processing and Refinement

All crystals were cryoprotected and flash frozen in liquid nitrogen-cooled liquid propane. Crystals were kept at  $-180^\circ\text{C}$  under a stream of boiled liquid nitrogen during data collection. Multiwavelength diffraction data used for solving the structure of the C222<sub>1</sub> crystal form by the MAD method were collected at the Cornell High Energy Synchrotron Source (CHESS) F2 station. Data for the P<sub>4</sub> crystal form were collected at the National Synchrotron Light Source (NSLS) X25 station (Brookhaven National Laboratory). All data were processed with DENZO and scaled with SCALEPACK (Otwinowski, 1993). The selenium sites were determined by direct methods and Patterson search using SHELX (Sheldrick, 1990). MLPHARE (CCP4, 1994) was used for refinement of the selenium sites and phase calculation. The electron density map was improved by solvent flattening using DM (Cowtan, 1994) and 2-fold averaging using RAVE (Kleywegt and Jones, 1994). The model was built with the program O (Jones et al., 1991), and model refinement was performed with CNS by iterative cycles of simulated annealing and model rebuilding (Brunger et al., 1998). The structure of the P<sub>4</sub> crystal form was determined by molecular replacement. Rotation and translation searches were performed by using AmoRe (Navaza, 1994). Both refined models contain residues from His-241 to Asn-393, and the last 24 residues (Ser-394 to Lys-417) are disordered.

### Mass Spectrometry

Maldi-time-of-flight mass spectrometry (PerSeptive Biosystems Voyager-STR) was used in analyzing the purified protein for crystallization (Cadene and Chait, 2000; Cohen and Chait, 2001). The measured mass indicates that the His tag of the protein was completely removed after thrombin cleavage and the starting methionine was cleaved during expression. Substitution of methionine with selenomethionine was quantified by mass spectrometry and confirmed to be essentially complete.

### Electrophysiology

All recording solutions share the following ingredients (in mM): 140 K gluconate (Fluka), 20 KCl (Fluka), 20 HEPES (pH 7.5), and 5 EGTA (Fisher). Free calcium ion concentration (Ca<sup>2+</sup>) was set by adding the amount of CaCl<sub>2</sub> (Fluka) determined by equilibrium calculations using  $3.86 \times 10^{-7} \text{ M}$  as the equilibrium constant for the formation of the EGTA-Ca<sup>2+</sup> complex. Appropriate mixtures of 1 mM Ca<sup>2+</sup> and 0  $\mu\text{M}$  (or  $< 2 \text{ nM}$ ) Ca<sup>2+</sup> solutions provided the four test solutions: 3, 5, 10, and 300  $\mu\text{M}$  Ca<sup>2+</sup>. The pipette solution consisted of the 3  $\mu\text{M}$  Ca<sup>2+</sup> solution with MgCl<sub>2</sub> added to  $\sim 2 \text{ mM}$  to improve seal formation.

Oocytes were dissected from *Xenopus laevis* frogs and treated with collagenase to remove the follicular layer. Treated oocytes were injected with about 50 nL of in vitro-transcribed RNA (50 ng) encoding wild-type or mutant constructs of the Human BK channel. Optimal expression levels were reached two to three days after RNA injection. Patch pipettes were pulled and fire polished to provide serial resistances between 1.1 and 2.3 M $\Omega$ . Maximum macropatch tail currents ranged from  $-1.5$  to  $-9.5 \text{ nA}$ , indicating that the number of channels ranged from 100 to 600. Patches were excised in the bath solution containing 3  $\mu\text{M}$  Ca<sup>2+</sup>. For each patch, two families of current traces were collected in each of the four calcium-buffered solutions. Bath solutions were exchanged by a gravity-flow apparatus feeding into a Warner laminar flow chamber (RC-24E). After patch excision, the solutions were exchanged in the following order

(Ca<sup>2+</sup> in  $\mu$ M): 300, 10, 5, 3, and 300. The first and last data sets (both in 300  $\mu$ M Ca<sup>2+</sup>) were used to calculate a linear time-dependent scaling function to compensate for the "run-down" phenomena commonly observed in patch-clamp studies of BK channels. Each patch experiment lasted between 20 and 30 min. Baseline and leak subtractions were made simultaneously from linear extrapolations of tail currents elicited by the initial four or five nonactivating voltage steps within each family of traces.

#### Acknowledgments

We thank members of the MacCHESS (F2) and Brookhaven National Laboratory (X25) staff for assistance in data collection and W. Chin for help in manuscript preparation. This work was supported by a grant to B. T. C. from the National Center for Research Resources (RR00862) and a grant to R. M. from the National Institutes of Health (47400). R. M. is an Investigator in the Howard Hughes Medical Institute.

Received December 19, 2000; revised January 17, 2001.

#### References

- Altschul, S.F., Madden, T.L., Schaffer, A.A., Zhang, J., Zhang, Z., Miller, W., and Lipman, D.J. (1997). Gapped BLAST and PSI-BLAST: a new generation of protein database search programs. *Nucleic Acids Res.* **25**, 3389–3402.
- Bellamacina, C.R. (1996). The nicotinamide dinucleotide binding motif: a comparison of nucleotide binding proteins. *FASEB J.* **10**, 1257–1269.
- Branden, C., and Tooze, J. (1991). Enzymes that bind nucleotides. In *Introduction to Protein Structure*, C. Branden and J. Tooze, eds. (New York: Garland Publishing), pp. 141–159.
- Brunger, A.T., Adams, P.D., Clore, G.M., DeLano, W.L., Gros, P., Grosse-Kuntze, R.W., Jiang, J.S., Kuszewski, J., Nilges, M., Pannu, N.S., et al. (1998). Crystallography & NMR system: a new software suite for macromolecular structure determination. *Acta Crystallogr. D. Biol. Crystallogr.* **54**, 905–921.
- Cadene, M., and Chait, B.T. (2000). A robust, detergent-friendly method for mass spectrometric analysis of integral membrane proteins. *Anal. Chem.* **72**, 5655–5658.
- CCP4 (collaborative computational project 4) (1994). The CCP4 suite: programs for protein crystallography. *Acta Crystallogr. D50*, 760–763.
- Cohen, S.L., and Chait, B.T. (2001). Mass spectrometry as a tool for protein crystallography. *Annu. Rev. Biophys. Biomol. Structure* **30**, 67–85.
- Cortes, D.M., and Perozo, E. (1997). Structural dynamics of the *Streptomyces lividans* K<sup>+</sup> channel (SKC1): oligomeric stoichiometry and stability. *Biochemistry* **36**, 10343–10352.
- Cowtan, K. (1994). DM: an automated procedure for phase improvement by density modification. *Joint CCP4 and ESF-EACBM Newsletter on Protein Crystallography* **31**, 34–38.
- Cserzo, M., Wallin, E., Simon, I., von Heijne, G., and Elofsson, A. (1997). Prediction of transmembrane  $\alpha$ -helices in prokaryotic membrane proteins: the dense alignment surface method. *Protein Eng.* **10**, 673–676.
- Cui, J., and Aldrich, R.W. (2000). Allosteric linkage between voltage and Ca(2+)-dependent activation of BK-type msl1 K(+) channels. *Biochemistry* **39**, 15612–15619.
- Derst, C., and Karschin, A. (1998). Evolutionary link between prokaryotic and eukaryotic K<sup>+</sup> channels. *J. Exp. Biol.* **201**, 2791–2799.
- Doyle, D.A., Morais Cabral, J.H., Pfuetzner, R.A., Kuo, A., Gulbis, J.M., Cohen, S.L., Chait, B.T., and MacKinnon, R. (1998). The structure of the potassium channel: molecular basis of K<sup>+</sup> conduction and selectivity. *Science* **280**, 69–77.
- Durell, S.R., Hao, Y., Nakamura, T., Bakker, E.P., and Guy, H.R. (1999). Evolutionary relationship between K<sup>+</sup> channels and symporters. *Biophys. J.* **77**, 775–788.
- Finn, J.T., Grunwald, M.E., and Yau, K.W. (1996). Cyclic nucleotide-gated ion channels: an extended family with diverse functions. *Annu. Rev. Physiol.* **58**, 395–426.
- Hille, B. (1992). *Ionic Channels of Excitable Membranes* (Sunderland, MA: Sinauer Associates).
- Jones, T.A., Zou, J.Y., Cowan, S.W., and Kjeldgaard, M. (1991). Improved methods for binding protein models in electron density maps and the location of errors in these models. *Acta Crystallogr. A.* **47**, 110–119.
- Keen, J.E., Khawaled, R., Farrens, D.L., Neelands, T., Rivard, A., Bond, C.T., Janowsky, A., Fakler, B., Adelman, J.P., and Maylie, J. (1999). Domains responsible for constitutive and Ca(2+)-dependent interactions between calmodulin and small conductance Ca(2+)-activated potassium channels. *J. Neurosci.* **19**, 8830–8838.
- Kleywegt, G.J., and Jones, T.A. (1994). From the first map to final model. In *Proceedings of the CCP4 Study Weekend*, S. Bailey, R. Hubbard, and D. Waller, eds. (Daresbury, UK: Daresbury Laboratory), pp. 59–66.
- Lee, J.O., Rieu, P., Arnaout, M.A., and Liddington, R. (1995). Crystal structure of the A domain from the alpha subunit of integrin CR3 (CD11b/CD18). *Cell* **80**, 631–638.
- Liu, Y., Holmgren, M., Jurman, M.E., and Yellen, G. (1997). Gated access to the pore of a voltage-dependent K<sup>+</sup> channel. *Neuron* **19**, 175–184.
- Milkman, R. (1994). An *Escherichia coli* homologue of eukaryotic potassium channel proteins. *Proc. Natl. Acad. Sci. USA* **91**, 3510–3514.
- Moss, G.W., Marshall, J., and Moczydlowski, E. (1996). Hypothesis for a serine proteinase-like domain at the COOH terminus of Slowpoke calcium-activated potassium channels. *J. Gen. Physiol.* **108**, 473–484.
- Navaza, J. (1994). AMoRe: an automated package for molecular replacement. *Acta Crystallogr. A50*, 157–163.
- Otwiniowski, Z. (1993). Oscillation data reduction program. In *Data Collection and Processing*, L. Sawyer, N. Isaacs, and S. Bailey, eds. (Daresbury, UK: Daresbury Laboratory), pp. 56–62.
- Paoletti, P., Perin-Dureau, F., Fayyazuddin, A. Goff, A.L., Callebaut, I., and Neyton, J. (2000). Molecular organization of a zinc binding N-terminal modulatory domain in a NMDA receptor subunit. *Neuron* **28**, 911–925.
- Parra-Lopez, C., Lin, R., Aspedon, A., and Groisman, E.A. (1994). A *Salmonella* protein that is required for resistance to antimicrobial peptides and transport of potassium. *EMBO J.* **13**, 3964–3972.
- Perozo, E., Cortes, D.M., and Cuello, L.G. (1999). Structural rearrangements underlying K<sup>+</sup>-channel activation gating. *Science* **285**, 73–78.
- Sack, J.S., Saper, M.A., and Quioco, F.A. (1989). Periplasmic binding protein structure and function. Refined X-ray structures of the leucine/isoleucine/valine-binding protein and its complex with leucine. *J. Mol. Biol.* **206**, 171–191.
- Sanchez, R., and Sali, A. (1998). Large-scale protein structure modeling of the *Saccharomyces cerevisiae* genome. *Proc. Natl. Acad. Sci. USA* **95**, 13597–13602.
- Schlosser, A., Hamann, A., Bossemeyer, D., Schneider, E., and Bakker, E.P. (1993). NAD<sup>+</sup> binding to the *Escherichia coli* K(+) uptake protein TrkA and sequence similarity between TrkA and domains of a family of dehydrogenases suggest a role for NAD<sup>+</sup> in bacterial transport. *Mol. Microbiol.* **9**, 533–543.
- Schreiber, M., and Salkoff, L. (1997). A novel calcium-sensing domain in the BK channel. *Biophys. J.* **73**, 1355–1363.
- Sheldrick, G.M. (1990). Phase annealing SHELX-90: direct methods for larger structures. *Acta Crystallogr.* **46**, 467–473.
- Stumpe, S., Schlosser, A., Schleyer, M., and Bakker, E.P. (1996). K<sup>+</sup> circulation across the prokaryotic cell membrane: K<sup>+</sup>-uptake systems. In *Handbook of Biological Physics*, W.N. Konings, H.R. Kaback, and J.S. Lolkema, eds. (New York: Elsevier Science B.V.), pp. 473–499.
- Thompson, J.D., Higgins, D.G., and Gibson, T.J. (1994). CLUSTAL W: improving the sensitivity of progressive multiple sequence align-

ment through sequence weighting, position-specific gap penalties and weight matrix choice. *Nucleic Acids Res.* *22*, 4673–4680.

Tucker, S.J., Gribble, F.M., Zhao, C., Trapp, S., and Ashcroft, F.M. (1997). Truncation of Kir6.2 produces ATP-sensitive K<sup>+</sup> channels in the absence of the sulphonylurea receptor. *Nature* *387*, 179–183.

Xia, X.M., Fakler, B., Rivard, A., Wayman, G., Johnson-Paid, T., Keen, J.E., Ishii, T., Hirschberg, B., Bond, C.T., Lutsenko, S., et al. (1998). Mechanism of calcium gating in small-conductance calcium-activated potassium channels. *Nature* *395*, 503–507.

Yellen, G. (1998). The moving parts of voltage-gated ion channels. *Q. Rev. Biophys.* *31*, 239–295.

Zagotta, W.N., and Siegelbaum, S.A. (1996). Structure and function of cyclic nucleotide-gated channels. *Annu. Rev. Neurosci.* *19*, 235–263.